

Article

Centaurus A: Hard X-ray and High-Energy Gamma-Ray Light Curve Correlation

Isak Delberth Davids ^{1,2,*} , Markus Böttcher ²  and Michael Backes ^{1,2} 

¹ Department of Physics, University of Namibia, Private Bag 13301, Windhoek 12010, Namibia; mbackes@unam.na

² Centre for Space Research, North-West University, Private Bag X6001, Potchefstroom 2520, South Africa; Markus.Bottcher@nwu.ac.za

* Correspondence: isak.davids@gmail.com

Received: 26 February 2019; Accepted: 27 March 2019; Published: 4 April 2019



Abstract: Centaurus A, powered by a 55 million solar mass supermassive black hole, has been intensively monitored in all accessible wavelength ranges of the electromagnetic spectrum. However, its very-high energy gamma (γ) ray flux (TeV photons), obtained from H.E.S.S. is relatively faint, hampering detailed light curve analyses in the most energetic energy band. Yet, the extensive long-term light curve data from *Fermi*-LAT and *Swift*-BAT (hard X-rays) allows for cross-correlation studies. We find a hint that X-ray emission from Centaurus A precedes the γ rays by 25 ± 125 days. If this lag is real and related to a $\gamma\gamma$ absorption effect in the broad-line region (BLR) around the central source, we can constrain the size of the BLR using light-travel time arguments. These are first results of extended light curve correlation studies between high-energy γ rays and X-rays from Centaurus A.

Keywords: active galactic nucleus; radio galaxy; Centaurus A; GeV γ -rays; TeV γ -rays; light curve; discrete correlation function

1. Introduction

Active galactic nuclei (AGN) are a type of galaxies hosting extremely luminous central regions that can outshine the entire galaxy. It is customarily accepted that these active central regions are powered by a super-massive black hole (SMBH). The SMBH accretes matter from its surroundings through an accretion disk around it. AGN are known to feature a relativistic outflow, in the form of jets, of charged particles traveling in a highly collimated flow that slams into the intergalactic matter forming large radio lobes at the ends.

AGN can be classified based on the observer's viewing angle [1] with respect to the AGN jet orientation. Radio galaxies (RGs) belong to the type of AGN for which the jet viewing angle with respect to our line of sight is relatively large in contrast to blazars for which this angle is small. A well known radio galaxy is Centaurus A (Cen A), which is the source of interest in this study.

In general, radio-loud AGN feature a broadband (from radio to γ rays) emission spectrum which is primarily attributed to non-thermal radiation. Two distinct peaks can be seen in such a spectral energy distribution (SED) where the lower energy peak (extending from radio to X-rays) is traditionally accepted as being due to synchrotron emission from relativistic electrons in the jets. In leptonic models, the second hump (from X-rays to γ rays) in the SED is attributed to inverse-Compton upscattering of a soft target photon field by the same relativistic jet electron population.

Amongst the basic components of the structure of a typical AGN, are the fast-moving high-density clouds surrounding the central engine (but external to the jet) and located closer to the central SMBH than the optically obscuring dust torus. Due to the broad emission lines from this region, observed primarily in the optical and ultraviolet, these components are referred to as the broad line regions

(BLRs) of the AGN (see [2] for a discussion on the possible origins of the BLR). The location of the BLR can be measured by the reverberation method employing the light travel time, the width of the emission line which in turn indicates the speed of the BLR clouds, and the observable temporal lag between the ionizing continuum radiation from the accretion disk and the line emission. The intense BLR radiation field is likely to be an efficient target photon field for $\gamma\gamma$ -absorption of high-energy (HE; $E \sim 0.1 - 100$ GeV) and / or very-high energy (VHE; $E \gtrsim 100$ GeV) γ -rays producing electron-positron (e^-e^+) pairs [3,4].

In this work, we report results of the time-series study using the discrete cross-correlation of light curves as applied to *Swift*-BAT X-ray and *Fermi*-LAT γ -ray long-term observations of the nearest radio galaxy, Cen A.

2. Centaurus A

The massive elliptical galaxy NGC 5128 (discovered in 1826, and also known as Cen A), is the closest radio galaxy, at a distance of 3.4 Mpc [5]. This source is centrally powered by a SMBH of mass $5.5 \times 10^7 M_\odot$ (see e.g., [6,7]). The giant radio lobes of Cen A subtend $\sim 10^\circ$ on the sky due to its proximity to Earth. This Fanaroff-Riley Type I [8] radio galaxy has been observed from radio to VHE γ rays, and is an ideal target for studying radio lobes and relativistic outflows.

Long-term multi-wavelength observations of Cen A from various astronomical facilities lead to high-quality long-term light curves in several wavebands across the electromagnetic spectrum.

The Spectral Energy Distribution of Cen A

Numerous extensive studies have so far been carried out on Cen A, aiming at characterizing the SED of the source (see e.g., [5,9–12]). As is seen with other active galaxies, the SED of Cen A is dominated by non-thermal radiative output originating mainly from synchrotron and inverse-Compton emission mechanisms.

In [9], the broadband SED of Cen A is reported, ranging from radio to VHE γ -rays modeled with various theoretical emission processes. A break in the γ -ray spectrum of the source indicating a spectral upturn above 2.4 GeV has been established [10]. This break is not well modeled using a single leptonic synchrotron self-Compton model. Recent results, from joint observations by H.E.S.S. and *Fermi*-LAT [11], show that the VHE data points are consistently above the HE power-law extrapolation of the γ -ray spectrum measured below the break. There is clear evidence for a second spectral component in VHE γ rays in the SED.

In the so-called one-zone model, one considers a single emission region (say a relativistic blob traveling along the jet) producing γ rays by electron-induced upscattering of low energy photons through the inverse-Compton process. The target low energy photon populations can be internal or external to the jet system. The single-zone models generally fail to reproduce the VHE γ ray data of Cen A.

Also shown in [9,12], one can invoke a second emission zone with differing input parameters to account for the VHE data points. Such a two-zone leptonic scenario has been recently employed by the *Fermi*-LAT and H.E.S.S. collaborations to fully explain the entire γ -ray spectrum of Cen A [11].

Alternatively, the hadronic explanation of the HE peak uses energetic protons (interacting with low-energy photons) that produce γ -rays after photo-pion production that leads to pion and muon decay processes (or from proton-synchrotron radiation). These hadronic models will typically require an input of rather large power in the proton population (see e.g., [13]), reaching $10^{47} - 10^{49}$ erg \cdot s $^{-1}$. The corresponding luminosity estimates are much lower, by even two or more orders of magnitude for leptonic models—this is essentially attributed to electrons radiating more efficiently.

A combination of leptonic and hadronic (leptohadronic) models has also been used in a successful reproduction of the HE tail of the SED of Cen A where the TeV component is considered as the emission from a relativistic proton population that interacts with the photons (photohadronic interaction) produced by the primary leptonic component [12].

$\gamma\gamma$ Absorption

The TeV photons that result from inverse-Compton scattering can again undergo interactions with soft photons from various photon fields producing electron-positron pairs. The target photon field can be external to the jet—in particular an intense photon population is provided by the BLR of an AGN. Other external regions with soft photons include the accretion disk, the dusty torus, the cosmic microwave background, and the extragalactic background light.

Due to the potentially large density of the BLR radiation field, it is possible that $\gamma\gamma$ absorption by the BLR radiation field produces a discernible spectral signature. Indeed, $\gamma\gamma$ absorption in the BLR of blazars has been considered by several authors, see e.g., [3,4,14], requiring that the γ -ray emission region must be located outside or at the outer edge of the BLR, as significant $\gamma\gamma$ absorption by the BLR can be avoided by having the γ -ray emission region outside the BLR.

3. Multi-wavelength Observations

To study the long-term activity of Cen A, we obtained contemporaneous data spanning about 6.8 years of hard X-rays and high-energy γ rays.

3.1. X-ray Data

Hard X-ray data (15–150 keV) from the Burst Alert Telescope (BAT) [15] on board the Neil Gehrels Swift Observatory was used to obtain a 6.8-year span light curve. While primarily designed for gamma-ray burst (GRB) detection and rapid triggering, BAT is an efficient hard X-ray monitor instrument [16,17]. These data are readily available from the BAT transient source online repository¹, and have been used herein to produce the light curve binned in 14 day bins in the period from MJD 54703.6 to MJD 57195.6 (i.e., between 8 August 2008 and 22 June 2015). The starting date of this time window is set by the mission operation date of the *Fermi*-LAT, and the ending date by the time of analyses in the year 2015.

3.2. HE Gamma-ray Data

High-energy γ -ray (100 MeV – 500 GeV) observations of Cen A that were contemporaneous to the *Swift*-BAT data, from the Large Area Telescope (LAT), the primary instrument on board the Fermi gamma-ray Space Telescope (Fermi) [18], were used to extract the γ -ray light curve. We employed the publicly available event reconstruction tool (*Fermi*-LAT Pass 8 event-level analysis) [19], which has been optimized for point-like sources after a comprehensive review of γ -ray event analysis. Released in 2015, Pass 8 is considered to be the event reconstruction and analysis realizing the full scientific potential of the instrument by increasing the effective area, improving the point spread function, and widening the energy range to which LAT is sensitive. We performed unbinned likelihood analysis (a maximum likelihood optimization technique) as described in the LAT Cicerone (see [20]) to obtain the light curve in the energy range 0.1 to 500 GeV within a 10° region of interest centered at the position of Cen A. The LAT science tools include all Pass 8 background models, such as the galactic diffuse emission and the extragalactic isotropic diffuse emission models.

Figure 1 shows the X-ray and γ -ray light curves produced as described above. The light curves span 6.8 years of observations, sampled in 14 day bins.

¹ The publicly available monitor web page, <http://swift.gsfc.nasa.gov/docs/swift/results/transients/>, provides light curves for astrophysical sources observed with *Swift*-BAT.

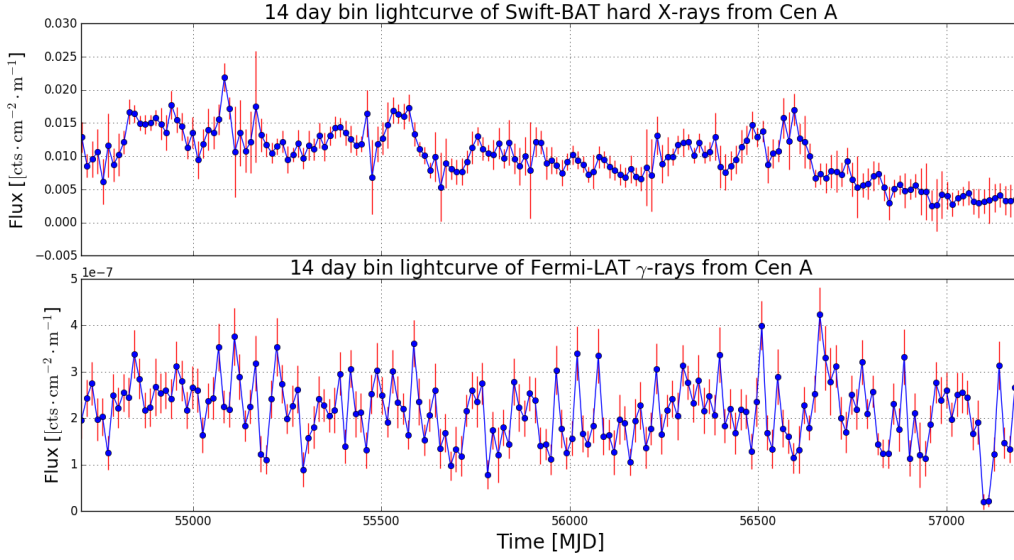


Figure 1. The Swift-burst alert telescope (BAT) and Fermi-large area telescope (LAT) light curves spanning 6.8 years between 2008 and 2015 (at a 14 day sample rate) is shown here.

4. Time-lag Analysis

4.1. The Discrete Correlation Function

We now test for the presence of a correlation (or absence thereof) between the two observed time varying signals from Cen A. For this purpose, we employ the discrete correlation function (DCF) analysis developed by [21]. One of the advantages of the DCF is that it does not interpolate data and can also handle sparse and / or unevenly sampled light curves.

Suppose we have recorded two time series of time-dependent data $a(t)$ and $b(t)$ (these can be in the form of astronomical fluxes), then the mathematical description of the set of unbinned discrete correlations is

$$UDCF_{ij} = \frac{(a_i - \bar{a})(b_j - \bar{b})}{[(\sigma_a^2 - e_a^2)(\sigma_b^2 - e_b^2)]^{1/2}}, \quad (1)$$

where a_i and b_j are observed flux pairs, such that the corresponding pairwise lag is $\Delta t_{ij} = t_j - t_i$. The averages of the series are denoted with \bar{a} and \bar{b} , while σ_a^2 and σ_b^2 represent their variances. The errors in these measurements are denoted by e_a and e_b . DCF values were computed for pairwise time-lags (M pairs in total) where each time-lag is given by $\Delta t_{ij} = t_j - t_i$. The DCF that we make use of here was then obtained through binning $UDCF_{ij}$ in time and averaging over all M pairs of $UDCF_{ij}$ for which $\tau - \Delta\tau/2 \leq |\Delta t_{ij}| \leq \tau + \Delta\tau/2$ to get

$$DCF(\tau) = \frac{UDCF_{ij}}{M}. \quad (2)$$

As can be seen in [21], the uncertainty in the DCF is obtained by

$$\sigma_{DCF}(\tau) = \frac{1}{M-1} \sqrt{\sum (UDCF_{ij} - DCF(\tau))^2}$$

where the summation is over all series of unbinned discrete correlations obtained in Equation (1).

The algorithm employed progressively iterates through time-lags and computes a discrete correlation coefficient for each lag. This enables an evaluation of the correlation between the two

time series as a function of difference in arrival time of the signals. The result can be interpreted as trailing or leading of the first input signal if the lag is positive or negative, respectively. The concept of auto-correlation is achieved if $a(t) = b(t)$.

4.2. Monte Carlo Simulation of Light Curves

In order to quantify the statistical significance of the DCF computed, we used the observed light curve in each band to simulate, via a Monte Carlo approach, a set of 20,000 artificial light curves. To accomplish this, an algorithm proposed by [22] and later improved by [23], was used. A Python implementation of this approach is published by [24].

For each observed light curve (the HE γ -ray and X-ray curves), we used the algorithm by [24] to extract the underlying power spectral densities (PSDs) and probability density functions (PDFs). These PSDs and PDFs are then used to simulate light curves that resemble the observations. At first, to get a PSD, the algorithm derives the associated periodogram (the power as function of frequency) which is in-turn fitted with a normalized (by A) smoothly bending power-law (around ν_{low} and ν_{high}) to which a constant c is added. Secondly, the PDF is obtained again from a best-fit (to its histogram) of a superposition of two distributions (a gamma-distribution $\Gamma(\kappa, \theta)$ and log-normal distribution $\ln N(\mu, \sigma^2)$) whose contributions are weighted by ω_{Γ} . The latter weighing takes care of the $\omega_{\ln N} = 1 - \omega_{\Gamma}$ partitioning of the mixing distributions towards the PDF. Table 1 shows the description and the numerical values of the above-mentioned parameters as used in this work.

Table 1. An illustration of the parameter set for simulating the γ -ray light curves in the Python implementation [24] of the algorithm by [23]. In this case, amongst others one, notes the over 80 % contribution of the Γ -distribution to the probability density function (PDF) at the expense of the log-normal component.

Parameter	Symbol	Numerical Value
PSD normalizer	A	0.03 Hz^{-1}
Bending frequency of PSD	ν_b	$2.3 \times 10^{-4} \text{ Hz}$
Low frequency slope in PSD	ν_{low}	1.1
High frequency slope in PSD	ν_{high}	2.2
Constant added for PSD	c	0.009
Shape parameter of Γ -distribution for PDF	κ	5.67
Scale parameter of Γ -distribution for PDF	θ	5.96
Mean of the log-normal distribution for PDF	ν	2.14
Variance of the log-normal distribution for PDF	σ^2	0.31
Weight between the Γ and log-normal distributions for PDF	ω_{Γ}	0.82

In this way, we simulated two pairs of 20,000 light curves resembling the γ -ray and the X-rays, respectively. We then obtained correlation coefficients (using the [21] framework) by correlating each of the 20,000 simulated light curves against the observed light curve in the other band. The simulated light curves feature the same variability and statistical properties as the observed light curves. Using the Monte Carlo simulated light curves, we sorted the lag-wise correlation coefficients and determined the upper 5% of these, which is used then to define the upper boundary of the 95% confidence level (CL). These limits derived from the contour boundaries of the CLs of the DCF process are used as a statistical significance check of the peak of the DCF distribution obtained.

4.3. DCF Computation Result

Figure 2 shows the discrete correlation function between hard X-rays and HE γ rays from Cen A. This is the correlation coefficient as a function of time-lag where the correlation was performed as described in Section 4.1. The shape of the peak in Figure 2 is approximately Gaussian for which the width is a measure of the uncertainty in the time lag. Overlaid on the correlation, is a band delimiting the 95% confidence level (see Section 4.2) which is significantly surpassed by the peak of the

correlation function. It can be noticed that the result hints to a scenario where the X-rays observed from the *Swift*-BAT instrument lead the *Fermi*-LAT γ -rays by 25 ± 125 days (see the peak of the Gaussian fit which has a *standard deviation* of 125 days). The correlation coefficient at the peak is 0.35 ± 0.14 . The result is established to have been significant above the 95% CL, but a correlation at a 99.7 CL significance cannot be claimed due to the magnitude of the error bars.

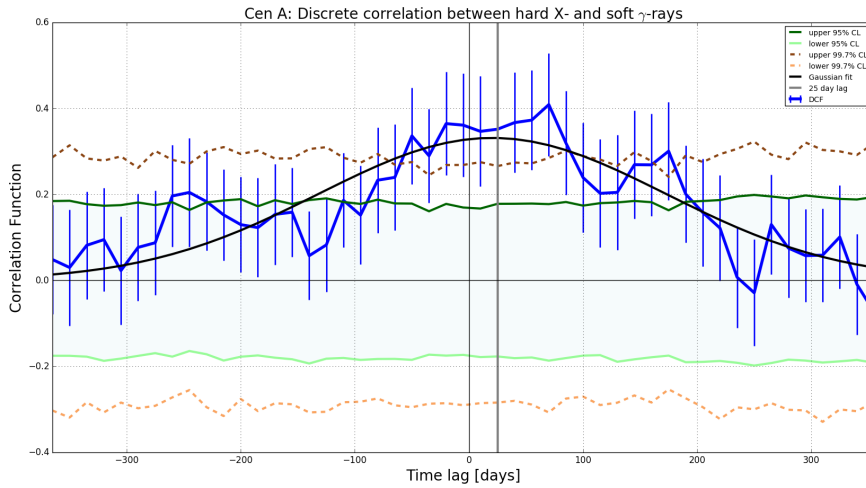


Figure 2. Discrete correlation function (DCF) result: the solid blue curve denotes the DCF as a function of time-lag (fitted with a Gaussian function in black), while the error bars on the correlation coefficients are propagated from the errors on the flux measurements. The peak at 25 ± 125 day time lag (indicated by the solid gray vertical line), is the deduced time-lag by which HE γ -rays trail behind the X-rays. The solid dark green line traces out the upper 95% confidence level (CL), while light green solid line marks the lower boundary of the 95% CL. Also shown are the upper and lower 99.7% CLs in dark brown and light brown, respectively. The lag bin width of the shown DCF is 15 days, constrained by the observation sampling rate and the duration of the observations. The latter also serves as a boundary to the lag range tested. This presented choice of the lag bin width and its range were arrived at by iterative visual inspection through these intervals. The correlation is insignificant on time scales larger than the time scale in this window.

5. Summary and Discussion

Cen A, the closest radio galaxy to Earth, has been observed in various wavelength bands across the electromagnetic spectrum over the years.

The light curve correlation between the 6.8 years of HE gamma-ray and the X-ray data of Cen A considered here, resulted in a hint of a possible time-lag of about 25 ± 125 days of the gamma-ray emission behind the X-rays. The discrete correlation function (DCF) associated with this lag peaked at the value of 0.35 ± 0.14 . Although the time-lag is a mere hint (due to the very broad Gaussian width of the peak), the correlation is above the 95% CL as obtained from the correlation studies done on the Monte Carlo simulated light curves.

In the event that further studies confirm a time-lag of this magnitude, then we can couple that to arguments of light-travel time, to set a constraint on the size of the BLR of the system. This is based on the argument that, while the emission region is within the BLR, X-rays produced by the relativistic particles escape immediately while γ rays are $\gamma\gamma$ absorbed. The resulting lag (t_{lag}) is then associated to the size of the BLR (R_{BLR}) through

$$\begin{aligned} \Delta R_{\text{BLR}} &\sim c \Delta t_{\text{lag}} \\ &\sim (6.5 \pm 32.4) \times 10^{16} \text{ cm.} \end{aligned}$$

This (25 light-day distance) would then indicate that the size of the BLR near the central engine is about 0.02 parsec. In this estimate, we neglect relativistic beaming for a typical radio galaxy for which the jet is largely misaligned to our line of sight.

Estimates of R_{BLR} of AGN have been set through a relationship with the observed luminosity of the accretion disk (see e.g., [25]) here written in the form of

$$R_{\text{BLR}} \sim 3 \times 10^{17} (L_{d45})^{1/2} \text{ cm},$$

where L_{d45} is the disk luminosity in units of 10^{45} erg/s. This relationship implies that AGN with luminosities in the range $10^{43} \text{ erg/s} \lesssim L_d \lesssim 10^{45} \text{ erg/s}$ feature BLR of sizes in the range of 12 to 116 light-days. This is consistent with the hint from the current work of the BLR in Cen A to be about 25 light-days.

Author Contributions: The formal analysis and the original draft preparation was carried out by I.D.D., while M.B. (Michael Backes) and M.B. (Markus Böttcher) contributed with validation, conceptualization, reviewing, editing and supervision. Furthermore, M.B. (Markus Böttcher) was pivotal in funding acquisition for the project.

Funding: This project is sponsored by the German Academic Exchange Service (DAAD) (German: Deutscher Akademischer Austauschdienst), the National Research Foundation²(NRF) and the Department of Science and Technology of the Republic of South Africa through the South African Research Chair Initiative under SARChI grant 64798, as well as the Department of Physics of the University of Namibia.

Conflicts of Interest: The authors declare no conflict of interest.

Abbreviations

The following abbreviations are used in this manuscript:

BAT	Burst Alert Telescope (on-board Neil Gehrels Swift Observatory)
BLR	Broad line region
CL	Confidence level
DCF	Discrete correlation function
HE	High-energy (gamma-rays of energy ~ 0.1 – 100 GeV)
H.E.S.S.	High-Energy Stereoscopic System
IACT	Imaging Atmospheric Cherenkov Telescope
LAT	Large Area Telescope (on-board Fermi satellite)
RG	Radio galaxy
SED	Spectral energy distribution
VHE	Very high-energy (gamma-rays of energy $\gtrsim 100$ GeV)

References

1. Urry, C.M.; Padovani, P. Unified Schemes for Radio-Loud Active Galactic Nuclei. *Publ. Astron. Soc. Pac.* **1995**, *107*, 803. [[CrossRef](#)]
2. Czerny, B.; Hryniewicz, K. The origin of the broad line region in active galactic nuclei. *Astron. Astrophys.* **2011**, *525*, L8. [[CrossRef](#)]
3. Roustazadeh, P.; Boettcher, M. Compton and Synchrotron Emission from Pair Cascades in Radio Galaxies. *AAS/High Energy Astrophys. Div.* **2011**, *12*, 4.08.
4. Böttcher, M.; Els, P. Gamma-Gamma Absorption in the Broad Line Region Radiation Fields of Gamma-ray Blazars. *Astrophys. J.* **2016**, *821*, 102–106. [[CrossRef](#)]
5. Israel, F.P. Centaurus A - NGC 5128. *Astron. Astrophys. Rev.* **1998**, *8*, 237–278. [[CrossRef](#)]

² Disclaimer: Any opinion, finding and conclusion or recommendation expressed in this material is that of the authors and the NRF does not accept any liability in this regard.

6. Marconi, A.; Pastorini, G.; Pacini, F.; Axon, D. J.; Capetti, A.; Macchetto, D.; Koekemoer, A.M.; Schreier, E.J. The supermassive black hole in Centaurus A: A benchmark for gas kinematical measurements. *Astron. Astrophys.* **2006**, *448*, 921–953. [[CrossRef](#)]
7. Häring-Neumayer, N.; Cappellari, M.; Rix, H.-W.; Hartung, M.; Prieto, M.A.; Meisenheimer, K.; Lenzen, R. VLT Diffraction-limited Imaging and Spectroscopy in the NIR: Weighing the Black Hole in Centaurus A with NACO. *Astrophys. J.* **2006**, *643*, 226–237. [[CrossRef](#)]
8. Fanaroff, B.L.; Riley, J.M. The morphology of extragalactic radio sources of high and low luminosity. *Mon. Not. R. Astron. Soc.* **1974**, *167*, 31P–36P. [[CrossRef](#)]
9. Abdo, A.A.; Ackermann, M.; Ajello, M.; Atwood, W.B.; Baldini, L.; Ballet, J.; Barbiellini, G.; Bastieri, D.; Baughman, B.M.; Bechtol, K.; et al. Fermi Large Area Telescope View of the Core of the Radio Galaxy Centaurus A. *Astrophys. J.* **2010**, *719*, 1433–1444. [[CrossRef](#)]
10. Graham, J.A.; Brown, A.M.; Boehm, C.; Lacroix, T.; Chadwick, P.M.; Joseph, S. The Fermi-LAT spectrum of Centaurus A—Analysis and interpretations. *AIP Conf. Proc.* **2017**, *1792*, 050004.
11. Abdalla, H.; Abramowski, A.; Aharonian, F.; Benkhali, F.A.; Angüner, E.O.; Arakawa, M.; Armand, C.; Arrieta, M.; Backes, M.; Balzer, A.; et al. The γ -ray spectrum of the core of Centaurus A as observed with H.E.S.S. and Fermi-LAT. *Astron. Astrophys.* **2018**, *619*, A71.
12. Petropoulou, M.; Lefa, E.; Dimitrakoudis, S.; Mastichiadis, A. One-zone synchrotron self-Compton model for the core emission of Centaurus A revisited. *Astron. Astrophys.* **2014**, *562*, A12. [[CrossRef](#)]
13. Böttcher, M.; Reimer, A.; Sweeney, K.; Prakash, A. Leptonic and Hadronic Modeling of Fermi-detected Blazars. *Astrophys. J.* **2013**, *768*, 54. [[CrossRef](#)]
14. Protheroe, R.J.; Biermann, P.L. Photon-photon absorption above a molecular cloud torus in blazars. *Astropart. Phys.* **1997**, *6*, 293–300. [[CrossRef](#)]
15. Gehrels, N.; Chincarini, G.; Giommi, P.; Mason, K.O.; Nousek, J.A.; Wells, A.A.; White, N.E.; Barthelmy, S.D.; Burrows, D.N.; Cominsky, L.R.; et al. The Swift Gamma-Ray Burst Mission. *Astrophys. J.* **2004**, *611*, 1005–1020. [[CrossRef](#)]
16. Krimm, H.A.; Barthelmy, S.D.; Markwardt, C.B.; Sanwal, D.; Tueller, J.; Gehrels, N.; Swift/BAT Team. The Swift-BAT Hard X-ray Transient Monitor. *Bull. Am. Astron. Soc.* **2006**, *38*, 374.
17. Krimm, H.A.; Holland, S.T.; Corbet, R.H.D.; Pearlman, A.B.; Romano, P.; Kennea, J.A.; Bloom, J.S.; Barthelmy, S.D.; Baumgartner, W.H.; Cummings, J.R.; et al. The Swift/BAT Hard X-Ray Transient Monitor. *Astrophys. J. Suppl. Ser.* **2013**, *209*, 14. [[CrossRef](#)]
18. Abdo, A.A.; Ackermann, M.; Althouse, W.; Anderson, B.; Axelsson, M.; Baldini, L.; Ballet, J.; Band, D.L.; Barbiellini, G.; et al. The Large Area Telescope on the Fermi Gamma-Ray Space Telescope Mission. *Astrophys. J.* **2009**, *697*, 1071–1102.
19. Atwood, W.; Albert, A.; Baldini, L.; Tinivella, M.; Bregeon, J.; Pesce-Rollins, M.; Sgrò, C.; Bruel, P.; Charles, E.; Drlica-Wagner, A.; et al. Pass 8: Toward the Full Realization of the Fermi-LAT Scientific Potential. *arXiv* **2013**, arXiv:1303.3514.
20. Abdo, A.A.; Ackermann, M.; Ajello, M.; Atwood, W.B.; Axelsson, M.; Baldini, L.; Ballet, J.; Band, D.L.; Barbiellini, G.; Bastieri, D.; et al. Fermi/Large Area Telescope Bright Gamma-Ray Source List. *Astrophys. J. Suppl. Ser.* **2009**, *183*, 46–66. [[CrossRef](#)]
21. Edelson, R.A.; Krolik, J.H. The discrete correlation function: A new method for analyzing unevenly sampled variability data. *ESA Spec. Public.* **1988**, *281*, 646–659. [[CrossRef](#)]
22. Timmer, J.; Koenig, M. On generating power law noise. *Astron. Astrophys.* **1995**, *300*, 707.
23. Emmanoulopoulos, D.; McHardy, I.M.; Papadakis, I.E. Generating artificial light curves: Revisited and updated. *Mon. Not. R. Astron. Soc.* **2013**, *433*, 907–927. [[CrossRef](#)]
24. Connolly, S. A Python Code for the Emmanoulopoulos et al. [[arXiv:1305.0304](#)] Light Curve Simulation Algorithm. *arXiv* **2015**, arXiv:1503.06676.
25. Bentz, M.C.; Peterson, B.M.; Netzer, H.; Pogge, R.W.; Vestergaard, M. The Radius-Luminosity Relationship for Active Galactic Nuclei: The Effect of Host-Galaxy Starlight on Luminosity Measurements. II. The Full Sample of Reverberation-Mapped AGNs. *Astrophys. J.* **2009**, *697*, 160. [[CrossRef](#)]

